1808 *Inorg. Chem.* **2011**, *50*, 1808–1815
DOI: 10.1021/ic102243c

Inorganic Chemistry
Article

$Ca_{14}Au_{46}Sn_5$: a "Colored" $Gd_{14}Ag_{51}$-Type Structure Containing Columns of Well-Differentiated Hexagonal Gold Stars

Qisheng Lin and John D. Corbett*

Department of Chemistry, Iowa State University, Ames, Iowa 50011, United States

Received November 8, 2010

A novel hexagonal phase discovered near the $Ca_{15}Au_{60}Sn_{25}$ quasicrystal and its cubic approximants (ACs) was synthesized by means of high-temperature solid-state reactions. Single-crystal structural analyses show that this is a $Gd_{14}Ag_{51}$ isotype with composition within the range $Ca_{14}Au_{45.56(4)-46.67(4)}Sn_{5.14(3)-4.14(3)}$, space group $P6/m$ (No. 175), and lattice parameters $a = 12.763(3)-12.879(3)$ Å and $c = 9.326(3)-9.3815(4)$ Å. In this phase, Sn mixes with Au in two of seven anionic sites to give a strong coloring that generates a narrow honeycomb-like Au/Sn template, in which sizable columns of hexagonal Au stars are confined. This phase transforms into the cubic 2/1 AC phase through a peritectic reaction at ~678 °C. The valence electron count per atom (e/a) of the present phase is in the range 1.41−1.45. However, it does not appear to follow a Hume−Rothery mechanism.

Introduction

Au-rich polar intermetallics[1] exhibit unprecedented and fascinating structures spanning from infinite one-dimensional (1D) tunnel structures,[2,3] through two-dimensional (2D) wavy Au sheets,[4] to aggregates of Au_4 tetrahedra[5,6] and numerous three-dimensional (3D) extended structures.[7−13] These, in turn, afford abundant opportunities to understand the relationships among the composition, structure, and bonding. The plethora of structural novelties originate, in part, from pronounced relativistic effects with Au,[14] which result in both greater 6s/5d orbital mixing and a slightly smaller effective metallic radius than its lighter congener Ag (1.439 vs 1.442 Å).[15] The relativistic effects also significantly enhance the Mulliken electronegativity for Au (5.77 eV)[16] and, ultimately, its binding with transition metals, p-block metalloids, and active alkali and alkali-earth metals.

Pronounced relativistic effects with Au also appear to play important roles in the formation of some quasicrystals (QCs) and corresponding approximants (ACs). For example, QC and/or ACs have been found in the Ca−Au−T (T = Ga,[17] In,[18] Ge,[19] Sn[20]) systems, in which the Au atomic percentages vary between ~50 and 65%. Notice that QCs form only in cases in which certain criteria are met, that is, matches between the atomic size and valence electron counts per atom (e/a) as required by the Hume−Rothery rules.[21,22] The availabilities of QC/ACs in these more extended ternary systems are apparently also related to the relativistic effects of dominant gold, which mutually offset the changes in radii and electronegativities from Ga (1.404 Å, 3.2 eV) to In (1.579 Å, 3.1 eV) to Ge (1.444 Å, 4.6 eV) and to Sn (1.623 Å, 4.3 eV).[15,16] In comparison, there are no reports of the existence of QC/ACs containing Au's neighbors Pt or Hg, although considerable relativistic effects have been noted in respective intermetallics.[23−25]

*To whom correspondence should be addressed. E-mail: jcorbett@iastate.edu.

(1) Corbett, J. D. *Inorg. Chem.* **2010**, *49*, 13.
(2) Li, B.; Corbett, J. D. *J. Am. Chem. Soc.* **2006**, *128*, 12392.
(3) Li, B.; Corbett, J. D. *Inorg. Chem.* **2007**, *46*, 2022.
(4) Lin, Q.; Corbett, J. D. *Inorg. Chem.* **2007**, *46*, 8722.
(5) Li, B.; Kim, S.-J.; Miller, G. J.; Corbett, J. D. *Inorg. Chem.* **2009**, *48*, 6573.
(6) Li, B.; Kim, S.-J.; Miller, G. J.; Corbett, J. D. *Inorg. Chem.* **2009**, *48*, 11108.
(7) Mueller, J.; Zachwieja, U. *Z. Anorg. Allg. Chem.* **2000**, *626*, 1867.
(8) Doering, W.; Schuster, H. U. *Z. Naturforsch.* **1980**, *35b*, 1482.
(9) Doering, W.; Seelentag, W.; Buchholz, W.; Schuster, H. U. *Z. Naturforsch.* **1979**, *34b*, 1715.
(10) Cordier, R.; Roehr, C.; Kussmann, D.; Hoffmann, R. D.; Poettgen, R. *Z. Anorg. Allg. Chem.* **2001**, *627*, 2053.
(11) Mazzone, D.; Marazza, R.; Riani, P.; Zanicchi, G.; Cacciamani, G.; Fornasini, M. L.; Manfrinetti, P. *CALPHAD: Comput. Coupling Phase Diagrams Thermochem.* **2009**, *33*, 31.
(12) Zachwieja, U. *J. Alloys Compd.* **1996**, *235*, 7.
(13) Lin, Q.; Corbett, J. D. *Inorg. Chem.* **2009**, *48*, 5403.
(14) Pyykkö, P. *Angew. Chem., Int. Ed.* **2002**, *41*, 3573.
(15) Pauling, L. *The Nature of the Chemical Bond*, 3rd ed.; Cornell University Press: Ithaca, NY, 1960; p 403.
(16) Pearson, R. G. *Inorg. Chem.* **1988**, *27*, 734.
(17) Lin, Q.; Corbett, J. D. *Inorg. Chem.* **2008**, *47*, 7651.
(18) Lin, Q.; Corbett, J. D. *J. Am. Chem. Soc.* **2007**, *129*, 6789.
(19) Lin, Q.; Corbett, J. D. *Inorg. Chem.* **2010**, *49*, 4570.
(20) Lin, Q.; Corbett, J. D. *Inorg. Chem.* **2010**, *49*, in press.
(21) Hume-Rothery, W. *J. Inst. Met.* **1926**, *35*, 295.
(22) Mizutani, U. In *The Science of Complex Alloy Phases*; Massalski, T. B., Turchi, P. E. A., Eds.; TMS (The Minerals, Metals & Materials Society): Warrendale, PA, 2005; pp 1−42.
(23) Karpov, A.; Nuss, J.; Wedig, U.; Jansen, M. *Angew. Chem., Int. Ed.* **2002**, *42*, 4818.
(24) Karpov, A.; Nuss, J.; Wedig, U.; Jansen, M. *J. Am. Ceram. Soc.* **2004**, *126*, 14123.

 Published on Web 01/21/2011

In this work, we report the structure of a novel Au-rich polar intermetallic phase discovered during Ca−Au−Sn QC/AC explorations.[20] The refined composition range of the phase is $Ca_{14}Au_{51-x}Sn_x$ ($x \cong 4.1-5.1$), with e/a (valence electrons per atom) $\sim 1.41-1.45$. The structure is an isotype of $Gd_{14}Ag_{51}$,[26] but the more selective reduction of Au by Sn produces clean columns of hexagonal Au stars confined in honeycomb-like mixed Au/Sn spacers.[27−29] In contrast, the few other ternary $Gd_{14}Ag_{51}$ examples, such as $R_{14}Cu_{51-x}Ga_x$ (R = Gd, Er), do not exhibit such strong differentiation.[30,31] Remarkably, the present phase decomposes into major amounts of the $Ca_{13}Au_{47.2}Sn_{28.1}$ 2/1 AC[20] during a differential thermal analysis (DTA) scan at higher temperatures, suggesting a possible starting place for future searches for new QC/AC systems.

Experimental Section

Materials and Syntheses. Pure elements used as starting materials were as-received calcium dendritic pieces (Aldrich-APL, 99.99%, surface cleaned with surgical blade), Au particles (Ames Laboratory, > 99.99%), and Sn foil (Alfa Aesar, 99.9%). These were weighed in a N_2-filled glovebox (H_2O < 0.1 ppm volume) and loaded into precleaned Ta tubes with one end already welded ($\Phi \sim 9$ mm × 25 mm). The other end of each Ta tube was then weld-sealed under Ar. Finally, the container was sealed in evacuated and baked SiO_2 jackets ($< 10^{-5}$ Torr).

The title phase was first seen as minor products after several reactions (Ca > 14 atom %; Au > 55 atom %) that were designed to locate a Ca−Au−Sn icosahedral quasicrystal (i-QC) and approximant crystals (ACs),[20] as listed in Table 1. Single-crystal diffraction revealed that the major product of reaction 4 had a composition of $Ca_{14}Au_{45.8}Sn_{4.9}$ and was isostructural with $Gd_{14}Ag_{51}$ ($P6/m$).[26] The only Au/Sn admixtures in this phase occur in two of seven independent anionic sites. Therefore, reactions of $Ca_{14}Au_{51-x}Sn_x$ (x = 0, 12, 16, 28) were run with the aim to see whether ordered variants were accessible or not and, of course, to check the phase width. The reactions were heated at 850 °C for 24 h, slowly cooled to 500 °C (or 620 °C for reaction 1 and 400 °C for reaction 5) at a rate of 5 °C/h, annealed there for 1−3 weeks, and then quenched into water (Table 1).

All products exhibit metallic luster and are inert to air at room temperature. Therefore, all later products were handled in air. Single crystals were selected from crushed products under a microscope; other bulk samples were ground into fine powders for X-ray phase analyses.

X-ray analyses. Powder diffraction data were collected on a Huber G670 Guinier camera equipped with an area detector and Cu Ka_1 (λ = 1.540 598 Å) radiation. Lattice parameters of the title phase (Table 1) were refined from 2θ values of eight strong and distinguishable peaks within 19−50° with the aid of *UnitCell*.[32]

Five single crystals (**1**, **2**, **3**, **S1**, and **S2**) from different reactions were selected for structure determinations and to check the phase widths. Room temperature intensity data were collected with the aid of a Bruker APEX CCD diffractometer equipped with monochromatized Mo Ka radiation (λ = 0.710 69 Å) in an ω scan mode over a $2\theta = \sim 3-57°$ range and with 10−30 s/frame. Data integration, Lorentz polarization, absorption, and other corrections were made with the aid of the *SAINT* subprogram included in the *SMART* software package.[33] Analyses of systematic absences and intensity distributions of reflections revealed primitive and 6/m symmetry, yielding candidate space groups $P3$, $P\bar{3}$, $P6$, $P\bar{6}$, and $P6/m$. However, only $P\bar{3}$ and $P6/m$ agree with the centrosymmetric statistics on the basis of $|E^2 - 1|$, and both gave essentially the same structural model after least-squares refinements. However, the higher symmetry space group $P6/m$ describes the structural model better, as suggested by the program *Platon*[34] and the following refinements. The possibility of a superstructure was also considered; however, no superlattice reflections were observed with longer exposure times (30 s). In the following, the structure solution of crystal **2** is selected as an example.

Direct methods in *SHELXTL*[35] and space group $P6/m$ yielded 10 independent sites, 3 with suitable interatomic separations for Ca−Au/Sn and others for Au/Sn−Au/Sn. So, they were temporarily assigned to Ca1−Ca3 and Au1−Au7, respectively. After several cycles of refinements, closer examination of the structure revealed that neighboring Au4 atoms would generate hexagonal rings with very short edges (~1.62 Å) surrounding the origin and equivalent sites. Meanwhile, the refined isotropic displacement parameters of the provisional Au4 (0.063 e/Å^2), Au6 (0.022 e/Å^2), and Au7 (0.035 e/Å^2) were obviously larger than the average of other Au atoms (0.014 e/Å^2). These indicate that the Au4 site could be partially occupied by Au, Sn, or a Au/Sn mixture, whereas Au6 and Au7 contained Au/Sn mixtures. They were assigned to Au4, Au/Sn6, and Au/Sn7 in subsequent refinements, during which the isotropic displacement parameters for all atoms became normal after the occupancies were allowed to vary.

The refinements of fractional Au4 alone yielded an occupancy value of about 0.455(6). The last value agrees well with those reported for single atoms in parallel sites in other $Gd_{14}Ag_{51}$-type structures, e.g., 0.49(2) in $Ce_{14}Cu_{51}$[36] and 0.47(3) in $Hf_{14}Cu_{51}$.[37] The occupation of a fractional Sn at the Au4 (6j) site was excluded because this occupancy was refined to 0.74(1), an unfavorable value considering its necessary disorder of the $(Au4)_3$ triad in the structure (below). Moreover, the interatomic distance (2.803 Å) within this triad is also too small compared with normal Sn−Sn pairs, e.g., in CaAuSn (2.968 Å),[38] Li_2AuSn_2 (2.962 Å),[39] K_3AuSn_4 (2.916 Å),[40] and KAu_4Sn_6 (2.899 Å).[41] The possibility of a Au/Sn mixture at the Au4 site, refined as 0.38/0.12(1) under a constrained total occupancy of 0.5, was also excluded because it results in greater antibonding according to crystal orbital Hamilton population (COHP) analyses (below).

The final refinement of **2**, with anisotropic displacement parameters, converged at R1 = 4.80% and wR2 = 11.55%. All residual peaks in the difference Fourier map are small, with differences < 0.3 e/Å^2 in order. The maximal and minimal peaks are +4.86 and −4.93 e/Å^2, both within 0.8 Å of Au atoms, signatures of poor absorption corrections for heavy atoms. The refined composition of crystal **2** is $Ca_{14}Au_{45.79(4)}Sn_{4.94(1)}$ or, normalized in percentages, $Ca_{21.6}Au_{70.7(3)}Sn_{7.7(3)}$. The data collection and

(25) Dai, J.-C.; Gupta, S.; Gourdon, O.; Kim, H.-J.; Corbett, J. D. *J. Am. Chem. Soc.* **2009**, *131*, 8677.
(26) Bailey, D. M.; Kline, G. R. *Acta Crystallogr.* **1971**, *27*, 650.
(27) Miller, G. J. *Eur. J. Inorg. Chem.* **1998**, *5*, 523.
(28) Lee, C.-S.; Miller, G. J. *J. Am. Chem. Soc.* **2000**, *122*, 4937.
(29) Miller, G. J.; Lee, C.-S.; Choe, W. In *Inorganic Chemistry Highlights*; Meyer, G., Naumann, D., Wesemann, L., Eds.; Wiley-VCH: Weinheim, Germany, 2002; pp 21−53.
(30) Belgacem, B.; Pasturel, M.; Tougait, O.; Potel, M.; Roisnel, T.; Ben Hassen, R.; Noel, H. *J. Alloys Compd.* **2009**, *478*, 89.
(31) Gumenyuk, R. V.; Kuz'ma, Y. B. *Inorg. Mater.* **2007**, *43*, 135.
(32) Holland, T. J. B.; Redfer, S. A. T. *Miner. Mag.* **1997**, *61*, 65.
(33) *SMART*; Bruker AXS, Inc.: Madison, WI, 1996.
(34) Spek, A. L. *J. Appl. Crystallogr.* **2003**, *36*, 7.
(35) *SHELXTL*; Bruker AXS, Inc.: Madison, WI, 2000.
(36) Allibert, C.; Wong-Ng, W.; Nyburg, S. C. *Acta Crystallogr., Sect. C* **1984**, *40*, 211.
(37) Gabathuler, J. P.; White, P.; Parthe, E. *Acta Crystallogr., Sect. B* **1975**, *31*, 608.
(38) Kussmann, D.; Hoffmann, R. D.; Poettgen, R. *Z. Anorg. Allg. Chem.* **1998**, *624*, 1727.
(39) Wu, Z.; Mosel, B. D.; Eckert, H.; Hoffmann, R. D.; Poettgen, R. *Chem—Eur. J.* **2004**, *10*, 1558.
(40) Zachwieja, U.; Mueller, J.; Wlodarski, J. *Z. Anorg. Allg. Chem.* **1998**, *624*, 853.
(41) Li, B.; Corbett, J. D. *Inorg. Chem.* **2008**, *47*, 3610.

Table 1. Some Reaction Compositions, Products, and Refined Lattice Constants for the Title Phase in the Ca−Au−Sn System

				lattice constants a and c (Å)[c]		
reaction	Ca/Au/Sn (atom %)	conditions[a]	products and estimated yields[b]	powder data	single-crystal data	crystal code
1	14.3/57.1/28.6	850/620	80% $P6/m$ + 10% Ta_3Sn + U_1	12.760(1), 9.322(1)	12.763(3), 9.326(3)	**1**
2	14.3/64.3/21.4	850/500	90% $Pa3$ + 10% $P6/m$		12.7946(4), 9.3643(4)	**S1**
3	14.5/60.1/25.4	850/500	92% $Pa3$ + 8% $P6/m$		12.812(2), 9.361(2)	**2**
4	20.0/60.0/20.0	850/500	70% $P6/m$ + 30% Pa3	12.815(1), 9.367(1)	12.829(3), 9.3692(4)	**S2**
5	20.0/55.0/25.0	850/400	80% $P6/m$ + 10% CaAuSn + U_2	12.873(1), 9.366(1)	12.879(3), 9.3815(4)	**3**
6	21.5/60.0/18.5	850/500	>98% $P6/m$	12.816(1), 9.370(1)		
7	21.5/53.8/24.6	850/500	70% $P6/m$ + 20% CaAuSn + U_3	12.867(1), 9.373(1)		
8	21.5/35.4/43.1	850/500	90% CaAuSn + U_2			

[a] Only the heating and annealing temperatures are listed here; for others, see the text. [b] $P6/m$, $Im3$ and $Pa3$ represent the title phase and 1/1 and 2/1 ACs, respectively. U_x denotes unidentified phase. The percentages were roughly estimated according to the observed peak intensities in powder patterns. [c] Lattice parameters from powder data were refined from the eight strongest peaks within 2θ = 19−50°, if discernible.

Table 2. Crystal Data and Structure Refinement for $Ca_{14}Au_{46.67(4)}Sn_{4.14(3)}$ (**1**), $Ca_{14}Au_{45.79(4)}Sn_{4.94(3)}$ (**2**), and $Ca_{14}Au_{45.56(4)}Sn_{5.14(3)}$ (**3**)

	1	**2**	**3**
formula	$Ca_{14}Au_{46.67(4)}Sn_{4.14(3)}$	$Ca_{14}Au_{45.79(4)}Sn_{4.94(3)}$	$Ca_{14}Au_{45.56(4)}Sn_{5.14(3)}$
e/a	1.41	1.45	1.46
fw	10244.92	10166.54	10144.98
space group, Z	$P6/m$, 1	$P6/m$, 1	$P6/m$, 1
unit cell (Å)			
a	12.763(1)	12.812(2)	12.879(1)
c	9.326(1)	9.361(2)	9.3815(9)
volume (Å^3)	1315.6(2)	1330.7(4)	1347.6(2)
d_{cal} (g/cm^3)	12.931	12.685	12.501
abs coeff (mm^{-1})	132.778	129.199	127.071
reflns coll/R_{int}	11584/0.1150	8438/0.0519	11872/0.0732
data/restraints/param	1147/0/63	1140/0/63	1176/0/63
GOF on F^2	1.037	1.191	1.112
R1/wR2			
$I > 2\sigma(I)$	0.0412/0.0896	0.0480/0.1155	0.0390/0.0991
all data	0.0569/0.0964	0.0536/0.1185	0.0459/0.1024
max/min residuals (e/Å^3)	4.461/−5.357	4.859/−4.934	5.183/−4.729

structural refinement parameters for crystals **1**−**3** are given in Table 2, and their refined atomic positions (standardized with TIDY[42]) and isotropic displacement parameters, in Table 3. Selected interatomic distances (< 3.5 Å) for crystal **2** are listed in Table 4. The data collection, structural refinement parameters, and detailed crystallographic data for **S1** and **S2** are given in Tables S1 and S2 in the Supporting Information, respectively. Other crystallographic data are available in the CIF outputs in the Supporting Information.

Electronic Structure Calculations. The densities-of-states (DOS) were calculated by means of the self-consistent, tight-binding, linear-muffin-tin-orbital (LMTO) methods in the local density and atomic sphere (ASA) approximations, within the framework of the density funtional theory method.[43−46] Because the program cannot handle disordered atoms, a defect-free model was built for a straightforward LMTO calculation. This was achieved on the basis of crystal **2** with the following modifications: First, the structure was transformed into the subgroup of $P\bar{6}$, in which two independent Au4 sites are generated [each defining a $(Au4)_3$ triad]. Second, one triad was omitted, and M6 and M7 sites were assigned to their major components Au (76%) and Sn (52%), respectively. A model with the formula "$Ca_{14}Au_{47}Sn_4$" was so generated, with an e/a of 1.40, close to the experimental range (1.41−1.45). ASA radii for atomic sites were scaled at the limitation of 18% maximum overlap between two neighboring atomic spheres, and one interstitial sphere was introduced accordingly. The ASA radii for Ca, Au, Sn, and an empty sphere were 3.46−3.72, 2.85−3.05, 3.05, and 1.56 Å, respectively. Reciprocal space integrations were carried out by means of the tetrahedron method. The basis sets were 3d/4s/(4p) for Ca, 6s/6p/5d/(5f) for Au, and 5s/5p/(4d) for Sn, with orbitals in parentheses downfolded.[47] Scalar relativistic effects were automatically included in the calculations. The band structure was sampled for 24 × 24 × 8 k points in the irreducible wedge of the Brillouin zone. COHP analyses were also performed to gain insight into the bonding properties.[48]

To probe the site preference of Sn in this structure, relative Muliken populations (MOPs) for an idealized $Ca_{14}Au_{51}$ model ($P\bar{6}$) were also tried with the aid of the program *CAESAR*.[49] However, the relative MOP data returned a biased value for Au4 because such a handling of the 6-fold disorder of the triads is insufficient.

Results and Discussion

Phase Width and Phase Stability. The title hexagonal phase $Ca_{14}Au_{46}Sn_5$ is a new ternary phase in the Ca−Au−Sn system, in which only CaAuSn (*Pnma*)[38] and, recently, $Ca_3(Au,Sn)_{19}$ ($Im\bar{3}$), $Ca_{13}(Au,Sn)_{76}$ ($Pa\bar{3}$), and the *i*-QC $Ca_{15}Au_{65}Sn_{20}$ phases have been reported.[20]

According to powder data, the refined lattice parameters of the present phase span from $a \sim 12.76$ Å and $c \sim 9.32$ Å for product of reaction 1 to $a \sim 12.87$ Å and

(42) Gelato, L. M.; Parthé, E. *J. Appl. Crystallogr.* **1987**, *20*, 139.
(43) Tank, R.; Jepsen, O.; Burkhardt, A.; Andersen, O. K. *TB-LMTO-ASA Program*, version 4.7; Max-Planck-Institut für Festkörperforschung: Stuttgart, Germany, 1994.
(44) Shriver, H. L. *The LMTO Method*; Springer-Verlag: Berlin, Germany, 1984.
(45) Jepsen, O.; Snob, M. *Linearized Band Structure Methods in Electronic Band-Structure and its Applications*; Springer Lecture Notes; Springer Verlag: Berlin, Germany, 1987.
(46) Anderson, O. K.; Jepsen, O. *Phys. Rev. Lett.* **1984**, *53*, 2571.
(47) Lambrecht, W. R. L.; Andersen, O. K. *Phys. Rev. B* **1986**, *34*, 2439.
(48) Dronskowski, R.; Blöch, P. *J. Phys. Chem.* **1993**, *97*, 8617.
(49) Ren, J.; Liang, W.; Whangbo, M.-H. *CAESAR for Windows*; Prime-Color Software Inc., North Carolina State University: Raleigh, NC, 1998.

Table 3. Atomic Coordinates and Equivalent Isotropic Displacement Parameters for $Ca_{14}Au_{46.67(4)}Sn_{4.14(3)}$ (**1**), $Ca_{14}Au_{45.79(4)}Sn_{4.94(3)}$ (**2**), and $Ca_{14}Au_{45.56(4)}Sn_{5.14(3)}$ (**3**).[a]

atom[b]	Wyckoff	symmetry	occupancy	*x*	*y*	*z*	U_{eq} (Å^2)[c]
Au1	12l	1	1	0.4431(1)	0.1169(1)	0.3335(1)	0.013(1)
			1	0.4448(1)	0.1175(1)	0.3366(1)	0.014(1)
			1	0.4463(1)	0.1178(1)	0.3383(1)	0.014(1)
Au2	12l	1	1	0.0652(1)	0.2661(1)	0.2345(1)	0.014(1)
			1	0.0663(1)	0.2678(1)	0.2332(1)	0.021(1)
			1	0.0681(1)	0.2692(1)	0.2332(1)	0.024(1)
Au3	6k	*m*...	1	0.2400(1)	0.0668(1)	$^1/_2$	0.015(1)
			1	0.2399(1)	0.0658(1)	$^1/_2$	0.020(1)
			1	0.2405(1)	0.0652(1)	$^1/_2$	0.019(1)
Au4	6j	*m*...	0.469(5)	0.1410(2)	0.0376(2)	0	0.013(1)
			0.455(6)	0.1411(2)	0.0384(3)	0	0.017(1)
			0.450(5)	0.1410(2)	0.0386(2)	0	0.017(1)
Au5	2c	−6...	1	$^1/_3$	$^2/_3$	0	0.027(1)
			1	$^1/_3$	$^2/_3$	0	0.028(1)
			1	$^1/_3$	$^2/_3$	0	0.027(1)
M6	12l	1	0.82/0.18(1)	0.1081(1)	0.4935(1)	0.1520(1)	0.014(1)
			0.76/0.24(1)	0.1066(1)	0.4926(1)	0.1523(1)	0.018(1)
			0.74/0.26(1)	0.1065(1)	0.4922(1)	0.1526(1)	0.018(1)
M7	4h	3...	0.52/0.48(2)	$^1/_3$	$^2/_3$	0.3011(3)	0.026(1)
			0.48/0.52(2)	$^1/_3$	$^2/_3$	0.2956(3)	0.027(1)
			0.49/0.51(2)	$^1/_3$	$^2/_3$	0.2959(3)	0.027(1)
Ca1	6k	*m*...	1	0.1274(5)	0.4635(5)	$^1/_2$	0.011(1)
			1	0.1289(5)	0.4651(5)	$^1/_2$	0.011(1)
			1	0.1289(5)	0.4653(5)	$^1/_2$	0.013(1)
Ca2	6j	*m*...	1	0.3875(8)	0.1199(6)	0	0.031(2)
			1	0.3915(8)	0.1226(7)	0	0.029(2)
			1	0.3933(7)	0.1235(6)	0	0.027(1)
Ca3	2e	6...	1	0	0	0.302(1)	0.010(2)
			1	0	0	0.303(1)	0.011(2)
			1	0	0	0.3030(9)	0.008(2)

[a] Parameters for crystals **1**−**3** are listed in sequence. [b] M denotes a Au/Sn mixture. [c] U_{eq} is defined as one-third of the trace of the orthogonalized U^{ij} tensor.

Table 4. Selected Interatomic Separations (Å) and ICOHP (eV/Bond Molecule) in Crystal **2**, $Ca_{14}Au_{45.34(2)}Sn_{5.67(2)}$[a]

bond	distance	ICOHP	bond	distance	ICOHP	bond	distance	ICOHP
Au1−Au1	3.060(2)	0.92	Au3−Au3	2.751(1)	1.37	Ca1−M6	3.301(2)	0.34
Au1−Au2	2.976(1)	0.95	Au4−Au4	2.803(5)	1.07	Ca1−M7	3.229(5)	0.51
Au1−Au2	3.111(1)	0.75	Au5−M6	2.994(1)	1.06	Ca2−Au1	3.231(2)	0.38
Au1−Au3	2.816(1)	1.18	Au5−M7	2.767(3)	1.72	Ca2−Au2	3.147(6)	0.50
Au1−M6	2.829(1)	1.27	M6−M6	2.833(2)	1.30	Ca2−Au2	3.265(7)	0.39
Au1−M6	3.102(1)	0.77	M6−M6	2.852(2)	1.45	Ca2−Au4	2.828(9)	1.07
Au1−Au7	2.831(1)	1.58	M6−M7	2.955(2)	1.06	Ca2−Au5	3.194(9)	0.45
Au2−Au2	3.095(1)	0.74	Ca1−Au1	3.087(5)	0.44	Ca2−M6	3.233(7)	0.44
Au2−Au3	2.917(1)	0.97	Ca1−Au1	3.135(5)	0.48	Ca2−M6	3.275(8)	0.44
Au2−Au3	2.961(1)	0.88	Ca1−Au1	3.138(5)	0.42	Ca2−M6	3.285(9)	0.37
Au2−Au4	2.864(2)	1.15	Ca1−Au2	3.353(4)	0.30	Ca3−Au2	3.163(2)	0.35
Au2−Au4	2.894(2)	1.13	Ca1−Au3	3.213(6)	0.33	Ca3−Au3	3.313(6)	0.33
Au2−M6	2.765(1)	1.66	Ca1−Au3	3.290(5)	0.28	Ca3−Au4	3.264(9)	0.33

[a] M denotes a Au/Sn mixture.

$c \sim 9.37$ Å for reaction 5 (Table 1). The product distributions for both reactions indicate that these are very close to the phase boundaries; therefore, the refined composition range of the five selected single crystals defines an approximate phase homogeneity of $Ca_{14}Au_{45.56(4)-46.67(4)}Sn_{5.14(3)-4.14(3)}$. Attempts to obtain the same types of phases with larger or smaller Sn atomic percentages failed (Table 1). The e/a value thereof is ∼1.41−1.45, distinctly smaller than that of $Ca_3Au_{14.4}Sn_{4.4}$, the 1/1 AC (∼1.72), $Ca_{13}Au_{47.2}Sn_{28.1}$, the 2/1 AC (∼2.10), and $Ca_{15}Au_{65}Sn_{20}$, the *i*-QC (∼1.90).[20] However, e/a is close to that of the parent $Gd_{14}Ag_{51}$ (1.43)[26] and other isostructural $RE_{14}X_{51}$ (RE = rare-earth-metal; X = Cu,[37] Ag,[50] Au[51]). Topologically, the decreased valence electrons caused by the replacement of trivalent RE by divalent Ca is compensated for by an increase in the proportion of monovalent X to tetravalent Sn, the signature of an electron compound.

As mentioned earlier, the present phase was first obtained as a byproduct of 2/1 AC syntheses. In fact, the same hexagonal type phases have also been found (according to powder data) in some other systems, e.g., $Yb_{14}Cd_{51}$[52] and $Ce_{14}(Au,Sn)_{51}$.[53] Surprisingly, the present phase transforms into the 2/1 AC $Ca_{13}Au_{47.2}Sn_{28.1}$

(50) McMaster, O. D.; Gschneider, K. A. J.; Venteicher, R. F. *Acta Crystallogr., Sect. B* **1970**, *26*, 1224.
(51) McMaster, O. D.; Gschneider, K. A. J.; Bruzzone, G.; Palenzona, A. *J. Less-Common Met.* **1971**, *25*, 135.
(52) Wu, D.; Ugurlu, O.; Chumbley, L. S.; Kramer, M. J. *Philo. Mag.* **2005**, *86*, 381.
(53) Kenzari, S.; Demange, V.; Boulet, P.; de Weerd, M. C.; Ledieu, J.; Dubois, J. M.; Fournée, V. *J. Phys.: Condens. Matter* **2008**, *20*, 095218.

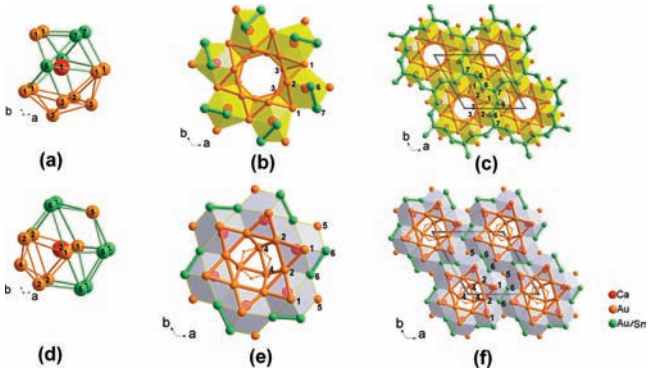

Figure 1. (a) Polyhedral environment of Ca1. (b) [001] view of the aggregation of six Ca1 polyhedra (shaded in yellow) into a gearlike wheel. (c) Fusion of Ca1 wheels into a layer normal to the *c* axis ($z = {}^1/_2$). (d) Polyhedral environment of Ca2. (e) Second wheel made of six Ca2 polyhedra (gray). Note that only one $(Au4)_3$ triad is shown within the central hexagonal cavity. The triad is 6-fold rotationally disordered to give small hexagonal rings (dashed lines). (f) Ca2 wheels fused into a layer normal to the *c* axis ($z = 0, 1$). Numbers mark the atomic sequence in Table 3.

and other unidentified minor phases through a peritectic reaction at ~678 °C during a fast DTA scan process (10 °C/min; Figure S1 in the Supporting Information). This encouraged us to check whether the present phase and the 2/1 AC have common icosahedral building blocks. However, icosahedral polyanionic clusters are scarce in this structural type (cf. Figure S2 in the Supporting Information), as opposed to the 2/1 AC. Therefore, examination of the temperature-dependent phase stabilities of some other $Gd_{14}Ag_{51}$-type phases might open new routes for QC/ACs.

Structural Description. According to single-crystal structural analyses, all five crystals investigated have very similar structural parameters (Tables 2, 3, and S1 and S2 in the Supporting Information) and are isotypic with $Gd_{14}Ag_{51}$,[26] a binary in which 3 of 10 independent sites are occupied by electropositive Gd and the remaining 7 by the more electronegative Ag. In the present structures, Ca topologically replaces Gd, Au/Sn (M) mixtures occupy two of the seven Ag sites, and Au alone fills the remaining five sites. For simplicity, the structure of $Ca_{14}Au_{45.79(4)}Sn_{4.94(3)}$ (**2**) with an intermediate composition and lattice parameters was chosen as an example for the structural description.

Figure 1 shows the coordination polyhedra of Ca1 and Ca2 and their aggregations. Each Ca1 has 14 neighbors: six Au1, two Au2, two Au3, two M6, and two M7, as shown in Figure 1a. These atoms define a polyhedron in which Au1, Au2, and Au3 atoms constitute a cluster unit of two interpenetrating pentagonal caps (Au bonds). This polyhedron exhibits a mirror plane symmetry, with Ca1 and Au3 atoms on the mirror plane normal to *c* ($z = {}^1/_2$). Because of a C_6 operation at $(0, 0, {}^1/_2)$, six Ca1 polyhedral clusters (yellow) share the Au1−Au1−Au3 triangular faces and aggregate into a gearlike wheel (Figure 1b). As a result, each wheel contains a larger hexagonal Au star (Au bonds). The innermost part of the star is a large hexagonal cavity defined by six Au3 atoms, whereas the vertices of the outward triangles are unexceptionally occupied by Au1, and the bases, by Au2 atoms. The $d_{Au3-Au3}$ distance is 2.751(1) Å, comparable to those in other Au-rich intermetallics, e.g., $K_{12}Au_{21}Sn_4$ (2.729 Å),[6] K_3Au_5Tl (2.767 Å),[5] $Ca_4Au_{10}In_3$ (2.759 Å),[4] and $Ca_3Au_8Ge_3$ (2.777 Å).[13] According to calculations (below), the Au3−Au3 pair has the largest ICOHP value among all Au−Au pairs (Table 4), suggesting strong bonding interactions. At the unit cell level, the wheels centered at $(0, 0, {}^1/_2)$ and equivalent sites fuse into a layer through sharing of the Au1−Au1−M7−M7 and Au1−Au1−Au1−Au1 faces (cf. Figure 1c). Note that the fusion of neighboring wheels results in a somewhat short distance (3.83 Å) for the Ca1−Ca1 pairs perpendicular to the Au1−Au1−Au1−Au1 square face. [There are no direct Au1−Au1 bonds in this face (Figure 1a).] However, the Ca1−Ca1 bonding interactions are negligible (ICOHP 0.08 eV/bond molecule). The fusion also means that the individual M6−M7 bonds in each wheel link into a cagelike network, as shown with the green bonds in Figure 1b.

Each Ca2 locates in a polyhedron with 13 vertices (2Au1 + 4Au2 + Au5 + 6M6) plus one Au4 at about half-occupancy (Figure 1d). The polyhedron also exhibits mirror plane symmetry normal to *c*, with Ca2, Au4, and Au5 atoms lying on the plane ($z = 0$). Similar to the Ca1 polyhedra, each Ca2 polyhedron shares two Au2−Au2−M6−M6 faces with like clusters to generate a second six-membered gearlike wheel (Figure 1e). This wheel contains a same-sized hexagonal Au star as in Figure 1b, and the decorations of the six outward triangles are the same too. That is, Au1 occupies all vertices and Au2 all bases of the large triangles in the star. However, the center of this wheel is occupied by a small hexagonal ring defined by Au4, which has impossibly short Au4−Au4 distances (1.62 Å). Because the occupancy of Au4 is ~50%, it is reasonable to consider the small hexagonal ring instead as two rotationally disordered $(Au4)_3$ triads in the *ab* plane, as shown in Figure 1e. This disordered triad feature is reflected by both its nominally short distance to the neighboring Ca2 (2.829 Å) and the enlarged U_{11} and U_{22} of Ca2 (U_{11}:U_{22}:U_{33} = 0.06:0.03:0.01). As a result, the ellipsoids of Ca2 and Au4 are nearly perpendicular each other (Figure S3 in the Supporting Information). The same ellipsoid phenomenon evidently also exists in the other $Gd_{14}Ag_{51}$-type structures refined from single-crystal data.[26,36,37] Similar to Ca1 wheels, the gear wheels of Ca2 polyhedral clusters fuse into layers at $z = 0$ or 1 via shared Au5−M6−M6 triangular and M6−M6−M6−M6 square faces (Figure 1f). Notice that the M6−M6 bonds in this layer seem to be isolated in Figure 1f; however, they are actually linked together by M7 from Ca1 layers (not shown).

Figure 2a shows the packing of the layers about Ca1 and Ca2 at the unit cell level. To better show the layered structural motif, some clusters are omitted on the top Ca2 layer. As shown, the alternative stacking of Ca1 and Ca2 layers, with aligned hexagonal cavities, results in the formation of 1D hexagonal tunnels extending along the *c* axis (rose) at the four cell edges parallel to the *c* axis. However, the tunnel is periodically modulated, with its smallest inside diameter at the $(Au4)_3$ triads ($z = 0$). Figure 2b shows the side view of this tunnel. Each segment of the tunnel actually consists of two face-shared Ca3 polyhedra, each of which is defined by six Au2, six Au3, and a $(Au4)_3$ triad capping the $(Au2)_6$ hexagonal

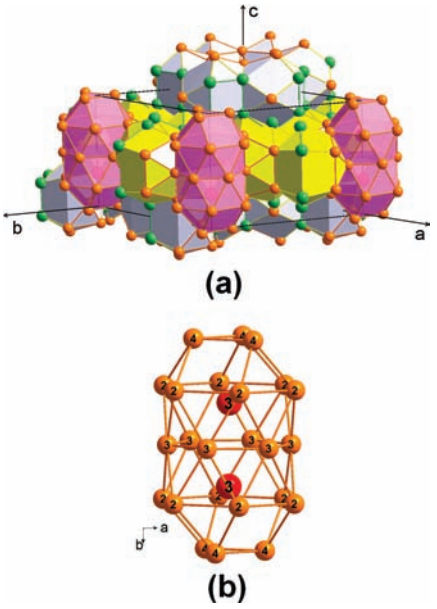

Figure 2. (a) Shaded polyhedral representation for $Ca_{14}Au_{46}Sn_5$ showing the layered structural motif. The layers made of Ca1 polyhedra (gray) locate at $z = 0$ and 1 and the layers of Ca2 polyhedra (yellow) at $z = 0.5$. The alternative stacking of Ca1 and Ca2 layers generates hexagonal tunnels (rose) along the cell edges parallel to *c*. For clarity, some polyhedra in the unit cell are omitted. The detailed Au structure within one of the former rose polyhedra is shown in part b. The color scheme is the same as that in Figure 1.

faces. Noteworthy is that the Au2 and Au3 atoms are those defining the hexagonal cavities in the Ca2 and Ca1 layers, respectively. The Ca3−Ca3 distance, 3.69 Å, is less than the sum of the Pauling metallic radii (3.94 Å); however, the bond interaction between the Ca3 pair is negligibly small, with ICOHP about 0.10 eV/bond molecule. Matrix effects and bonding within the Au network play a dominant role.

Recently, Tkachuk and Mar[54] reinvestigated the structures of $A_{14}Hg_{51}$ (A = Ca, Sr), which were formerly assumed to be isostructural with $Gd_{14}Ag_{51}$. According to their low-temperature (80 K) single-crystal data, they reformulated $A_{14}Hg_{51}$ as $A_{11-x}Hg_{54+x}$ ($x = 0.08$ for Ca and 0.52 for Sr) and solved the structure in space group $P\bar{6}$. As a result, the triads are ordered in the mercurides, and the hexagonal faces capped by the triads are slightly buckled such that all short distances are avoided. It would be interesting to analyze whether the ordering remains at room temperature in the mercurides and whether similar ordering of the triads occurs in other $Gd_{14}Ag_{51}$-type phases at low temperature.

Site Preference. Viewed along the *c* direction (Figure 1c, f), the Au/Sn mixed atoms (green) formally behave as spacers between the Au hexagonal stars in the Ca1 and Ca2 polyhedral layers. Actually, this is better seen when all shaded polyhedra are eliminated, and the bonds between hexagonal Au stars and the M spacers are deemphasized as narrow gray bonds (Figure 3). Now the structure is seen as columns of hexagonal Au stars confined in a honeycomb-like template of mixed Au/Sn and Au5 atoms. The detail of a column of the hexagonal star is shown in Figure S5 in the Supporting Information. It actually consists of the cluster shown in Figure 2b plus Au1 vertices in Figure 1a,b. Each Au3 at the waist of the star caps two interpenetrating pentagonal faces (one is shown in Figure S4 in the Supporting Information). As shown in Figures 1d−f, Au5 atoms are not members of the hexagonal stars, and they do not have bonding interactions with any Au atoms in the hexagonal stars (Table 4). In contrast, they lie directly below M7 atoms (cf. Figure S2e in the Supporting Information) and have strong interactions with only M6 and M7. In this sense, Au5 atoms also act as spacers. The well-differentiated structural pattern in Figure 3 suggests that Au sites, when mixed with Sn, are selectively reduced. Noteworthy is that no other $Gd_{14}Ag_{51}$-type ternary derivatives ($Er_{14}Cu_{40}Ga_{11}$,[30] $Gd_{14}Cu_{48}Ga_3$, and $Tb_{14}Cu_{48}Ga_3$[31]) have been as well-refined, so the question of site preference or "coloring"[27] is germane.

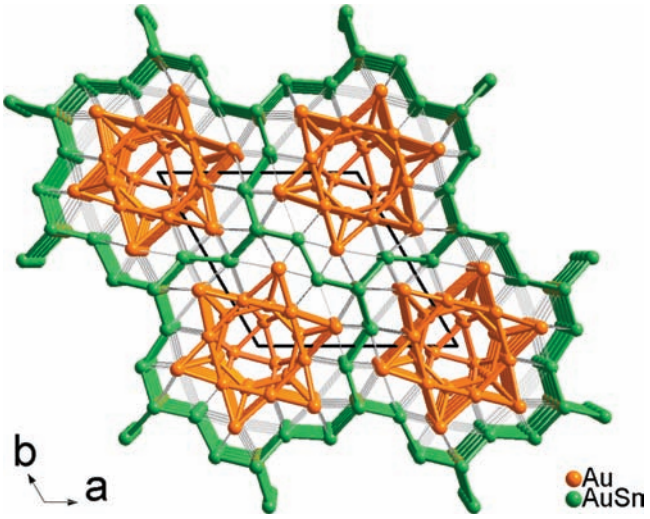

Figure 3. Perspective view of the polyanionic structure of $Ca_{14}Au_{46}Sn_5$ projected along the *c* axis, with emphasized Au−Au bonds (gold) in the hexagonal stars and the Au/Sn−Au/Sn bonds (green) in honeycomb-like spacers. All bonds between columns and spacers are deemphasized with small gray lines. One triad is shown at the center of each hexagonal star, and all Ca atoms are omitted for clarity.

Systematic Structural Changes. Figure 4 shows the variations of (a) lattice parameters and (b) percentages of Au at Au4, M6, and M7 sites as a function of e/a. Figure 4a shows how the *a* and *c* parameters increase over the sequence **1**, **S1**, **2**, **S2**, to **3** with an increased e/a, or the observed increase of Sn over Au in the respective formulas. The changes are ascribed to the different Au/Sn proportions: The greater the proportion of electron-richer Sn (1.623 vs 1.439 Å for Au),[15] the greater e/a and the larger the lattice parameters. However, variations of the *a* and *c* axes are not linear; the change in the *a* axis is larger than that in the *c* axis (inset in Figure 4b).

The nonlinear changes of the *a* and *c* parameters result from the following factors. In one aspect, as shown in Figure 2, the spacer atoms M6 form triangles in the *ab* plane and M7 locates above or below this plane; thus, a size change for M6 has a more pronounced effect in the *ab* direction, and a change of the M7 size, in the *c* dimension. This agrees well with the observation shown in Figure 4b, in which variations of Au atom % (or of Sn aom %) at the M6 sites are greater than those at M7, in the order **1**, **S1**, **2**,

(54) Tkachuk, A. V.; Mar, A. *Inorg. Chem.* **2008**, *47*, 1313.

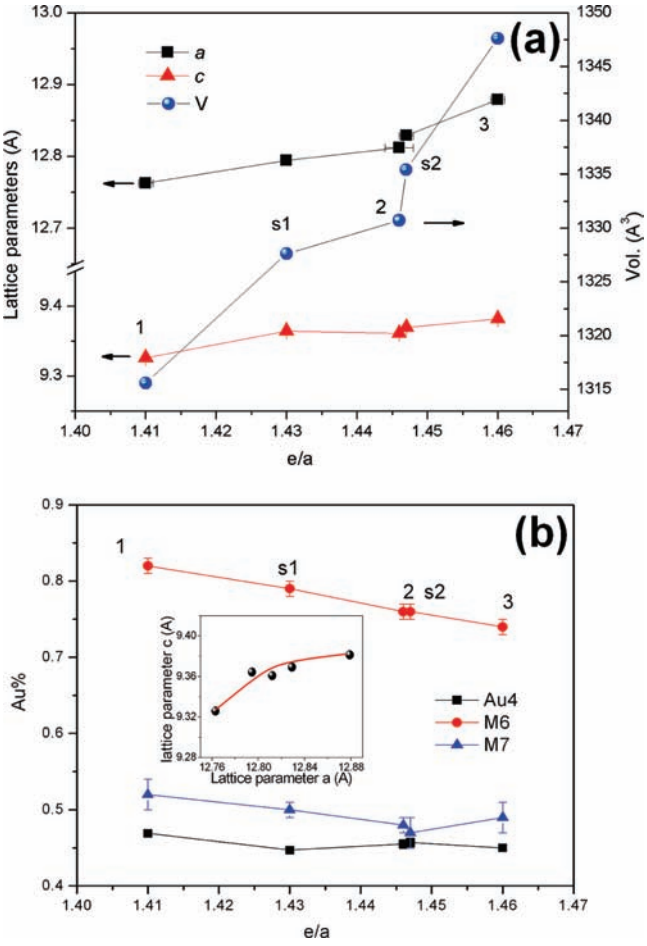

Figure 4. Variations of (a) lattice parameters and unit cell volumes and (b) the occupancies of Au in Au4, Au/Sn6, and Au/Sn7 sites as a function of e/a in five crystals. The inset in part b shows the nonlinear variation between *a* and *c*.

S2, to **3**. From another aspect, as Sn increases from **1**, **S1**, **2**, **S2**, to **3**, all Au−Au bond distances in the *ab* plane (Au1−Au2, Au1−Au3, Au3−Au3, and Au4−Au4) in the hexagonal Au stars increase, whereas those parallel to the *c* axis ($d_{Au1-Au1}$ and $d_{Au2-Au2}$) decrease. For example, the Au1−Au1 bond distances gradually decrease from 3.106 Å in **1** to 3.034 Å in **3**, whereas the Au2−Au2 distances increase from 3.066 to 3.122 Å.

Nevertheless, variations of the Au or Sn percentage at both M6 and M7 sites are small, as indicated by the slopes of both representative lines in Figure 4b. If both lines are extended, e/a of about 1.9−2.0 would be extrapolated for Au = 0%, at which point both M6 and M7 would contain only Sn. However, this e/a region is well beyond the range in which the present phase is stable (1.41−1.45). This is consistent with experimental failures to obtain a larger phase width.

Electronic Structure. Figure 5 shows (a) the DOS and (b and c) the average COHP data for the hypothetical "$Ca_{14}Au_{47}Sn_4$" (e/a = 1.4, Sn at M7 sites and Au at M6 sites). The total DOS pattern shows the characteristics of many polar intermetallic compounds.[55] Although the s and p states of Ca and p of Au and Sn spread over

(55) Gourdon, O.; Gout, D.; Miller, G. J. In *Encyclopedia of Condensed Matter Physics*; Bassani, B. S., Liedl, G., Wyder, P., Eds.; Elsevier: New York, 2005; pp 409−422.

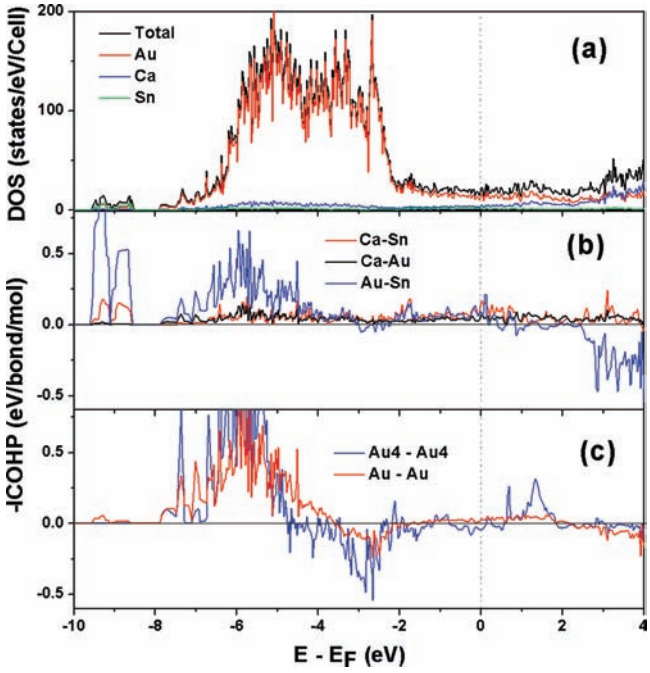

Figure 5. (a) Total and projected DOS and (b) the average Ca−Au, Ca−Sn, and Au−Sn bond and (c) the average Au−Au and Au4−Au4 bond COHP data for a hypothetical $Ca_{14}Au_{47}Sn_4$.

the whole energy range (Figure S5 in the Supporting Information), the s states of Sn and Au locate mainly in the energy ranges of −9.5 to −8.5 eV and −9.5 to −6.0 eV, respectively. Also, the many Au 5d states mainly populate the −7.0 to −2.0 eV range, with a small fraction extending to the Fermi energy (E_F) and above. Judging from the COHP data (Figure 5b), the interactions of the Au s and Sn s states give strong σ bonding within the range of −9.5 to −8.5 eV, whereas the predominant states between −8.0 and −2.0 eV are mainly the bonding and antibonding interactions among Au d, Sn p, and Ca s and p orbitals. The Ca 3d states are predominant above E_F (~5.0 eV), but some states spread well below E_F to interact with Au and Sn; however, the Ca−Au and Ca−Sn interactions are much weaker than those for Au−Au and Au−Sn, as suggested by the ICOHP data in Table 4. As for the major Au−Au bonding (Figure 5c), the average COHP data (eV/bond molecule) show strong bonding character within the energy ranges of −8.0 to −4.0 eV and −2.0 to +2.0 eV, but it is antibonding between −4.0 and −2.0 eV. Although the average Au−Au bond exhibits bonding character at the Fermi energy, E_F locates on a declining curve with Au4−Au4 antibonding character. Under rigid band assumptions, E_F will shift to the left if the Au4 sites contain some Sn contributions (the Au $5d^{10}$ electron is considered in the calculation; thus, it is electron-"richer" than Sn). That is, Au/Sn mixtures at the Au4 sites could result in a less stable state with stronger antibonding interactions, consistent with the structural analyses (above).

The stable e/a range for the present phase is narrow (1.41−1.45), and the values are close to those of typical Hume−Rothery phases.[21] However, the last generally exhibit pseudogaps around the Fermi level in DOS patterns that result from coincidences of the Fermi sphere and certain Brillouin zones in reciprocal space.[22] This is

apparently not the case for the hypothetical $Ca_{14}Au_{47}Sn_4$ (Figure 5), the Brillouin zone of which was sampled at 970 *k* points to be sure.

Conclusion

A new $Gd_{14}Ag_{51}$-type ternary phase has been discovered and structurally characterized, $Ca_{14}Au_{51-x}Sn_x$ (x = 4.1−5.1). The small phase width parallels selective mixing of Sn in only $^2/_7$ heavy-atom (Au) sites. This selective reduction of the anionic Au lattice yields an unprecedented novelty in this structure type: well-defined columns of Au stars in a honeycomb-like Au−Sn template. The large relativistic effects in Au bonding and its parallel large electronegativity are considered of primary importance.

The presence of three crystallographically distinct sites for the active metal in this structural type may be useful in order to introduce magnetic ordering; antiferromagnetic ordering has been noted even for the binary intermetallic $Tb_{14}Ag_{51}$, etc.[56]

(56) Fischer, P.; Pomjakushin, V.; Keller, L.; Daoud-Aladine, A.; Sikora, W.; Dommann, A.; Hulliger, F. *Phys. Rev. B* **2005**, *72*, 134413.

Although some $Gd_{14}Ag_{51}$-type ternary phases are available in QC systems, it is remarkable that the present phase transforms, in part, into the known 2/1 AC Ca−Au−Sn phase during a DTA scan. Some other $Gd_{14}Ag_{51}$-type phases might be useful jumping-off places for new QC searches.

Acknowledgment. We thank G. J. Miller for fruitful discussions on the site preference problems and Hume−Rothery mechanisms. This research was supported by the U.S. National Science Foundation, Solid State Chemistry, via Grant DMR-0853732. All of the work was performed in the facilities of the Ames Laboratory, U.S. Department of Energy.

Supporting Information Available: Tables S1 and S2 for the structural refinements and crystal data of crystals **S1** and **S2**, Figure S1 for powder patterns before and after a DTA scan, Figure S2 for detailed polyhedral environments of all Au and Au/Sn atoms, Figure S3 for a detailed gearlike wheel design of Ca2 polyhedral clusters, Figure S4 for the details of a hexagonal Au star, Figure S5 for projected DOS patterns, and CIF data for five crystals. This material is available free of charge via the Internet at http://pubs.acs.org.